Global Change Biology

Global Change Biology (2010) **16**, 255–271, doi: 10.1111/j.1365-2486.2009.01921.x

Evaluating the impacts of climate and elevated carbon dioxide on tropical rainforests of the western Amazon basin using ecosystem models and satellite data

HIROFUMI HASHIMOTO*†, FORREST MELTON*†, KAZUHITO ICHII‡, CRISTINA MILESI*†, WEILE WANG*† and RAMAKRISHNA R. NEMANI†

California State University, Monterey Bay, Seaside, CA 93955, USA, †NASA Ames Research Center, Moffett Field, CA 94035, USA, ‡Faculty of Symbiotic Systems Science, Fukushima University, Fukushima, Japan

Abstract

Forest inventories from the intact rainforests of the Amazon indicate increasing rates of carbon gain over the past three decades. However, such estimates have been questioned because of the poor spatial representation of the sampling plots and the incomplete understanding of purported mechanisms behind the increases in biomass. Ecosystem models, when used in conjunction with satellite data, are useful in examining the carbon budgets in regions where the observations of carbon flows are sparse. The purpose of this study is to explain observed trends in normalized difference vegetation index (NDVI) using climate observations and ecosystem models of varying complexity in the western Amazon basin for the period of 1984–2002. We first investigated trends in NDVI and found a positive trend during the study period, but the positive trend in NDVI was observed only in the months from August to December. Then, trends in various climate parameters were calculated, and of the climate variables considered, only shortwave radiation was found to have a corresponding significant positive trend. To compare the impact of each climate component, as well as increasing carbon dioxide (CO_2) concentrations, on evergreen forests in the Amazon, we ran three ecosystem models (CASA, Biome-BGC, and LPJ), and calculated monthly net primary production by changing a climate component selected from the available climate datasets. As expected, CO_2 fertilization effects showed positive trends throughout the year and cannot explain the positive trend in NDVI, which was observed only for the months of August to December. Through these simulations, we demonstrated that the positive trend in shortwave radiation can explain the positive trend in NDVI observed for the period from August to December. We conclude that the positive trend in shortwave radiation is the most likely driver of the increasing trend in NDVI and the corresponding observed increases in forest biomass.

Keywords: Amazon, ecosystem model, NDVI, NPP

Received 19 November 2008 and accepted 23 January 2009

Introduction

The dynamics of the evergreen forests in the Amazon basin have a substantial impact on worldwide climate systems and play an important role in the regulation of atmospheric carbon dioxide (CO_2) concentrations. Therefore, understanding the response of the Amazonian evergreen forests to climate change is critical for predicting the future global climate (Cramer *et al.*, 2004). Early numerical modeling studies for this region focused on the impact of deforestation on regional climate change and predicted that deforestation would have irreversible effects (by decreasing both precipitation and evapotranspiration) on the basin's hydrologic cycle (Salati & Vose, 1984). Along with the impacts of deforestation, it is expected that the response of the Amazonian forests to climate change accompanied by elevated CO_2 concentrations is the most important factor for

Correspondence: Hirofumi Hashimoto, California State University, Monterey Bay, Seaside, CA 93955, USA, tel. +1 650 604 6446, fax +1 650 604 6569, e-mail: hirofumi.hashimoto@gmail.com

Published 2009

predicting the future carbon balance of these ecosystems (Malhi, 2008). To assess the effect of these anthropogenic and climatological influences on future Amazon ecosystems, it is crucial to understand the mechanisms regulating the current state of the carbon balance and hydrologic cycles of the Amazon basin. Despite large uncertainty due to the insufficient number of observations over such a large region, a number of studies of the Amazon carbon balance have shown that these tropical evergreen forests have been sequestering carbon for the last two decades (see the review paper by Ometto *et al*., 2005). An intercomparison study of atmospheric CO_2 transportation models [the Atmospheric Tracer Transport Model Intercomparison Project (Transcom)] showed, although with large uncertainty in the estimates, that during the 1990s the carbon balance of tropical South America was almost neutral, while South America as a whole served as a small source of CO_2 (Gurney *et al*., 2002). This result implied that the evergreen forest ecosystems of the Amazon must function as carbon sinks to offset carbon emissions resulting from land-use change and fire (Houghton *et al*., 2000). Other plot-based studies provided proof that forest biomass has been increasing in the Amazon basin for the last few decades (Baker *et al*., 2004; Lewis *et al*., 2004b; Phillips *et al*., 2004), indicating that these evergreen forest ecosystems sequestered carbon in most of the Amazon basin. Also, measures of net ecosystem exchange using eddy covariance techniques revealed that carbon uptake was occurring at many sites [e.g. Reserva Jaru (Grace *et al*., 1995), Reserva Biológica do Cuieiras (Malhi *et al*., 1998), and Caxiuaña (Carswell *et al*., 2002), except for Tapajós (Saleska *et al*., 2003)].

Optical remote sensing and ecosystem model intercomparison are viable tools for deriving estimates of the amount of vegetation, and clarifying the driving mechanism and flows of carbon in regions where a limited number of carbon exchange observations are available. Satellite-based measures of vegetation density over vast areas can be derived through vegetation indexes such as the normalized difference vegetation index (NDVI) from the Advanced Very High Resolution Radiometer (AVHRR) satellite instrument, for which a global long-term record is available since 1981. However, optical remote sensing observations of tropical evergreen forests are complicated by residual cloud contamination (even after monthly compositing procedures are applied) and by the saturation of the band reflectance for regions with very dense vegetation, and require independent validation through the use of ecosystem models or field measurements.

Although a number of intercomparison studies of ecosystem carbon models have been performed at the global scale (Cramer *et al*., 1999), there are only few regional modeling studies for the tropics which are based on individual models. Early ecosystem model-based studies of the Amazon basin found that net primary production (NPP, the net amount of carbon fixed in vegetation by the photosynthetic process) was sensitive to changes in soil moisture resulting from variability in precipitation, and that heterotrophic respiration increased with temperature (Tian *et al*., 1998). Recently, both diagnostic (Nemani *et al*., 2003; Hicke, 2005) and prognostic (Ichii *et al*., 2005) ecosystem models reported that the carbon budget of the Amazon basin is more sensitive to the interannual variation in shortwave radiation. For example, the Biome-BGC results of Ichii *et al*. (2005) indicated that the interannual variability in gross primary production (GPP, the amount of carbon absorbed by photosynthesis discounted for carbon lost through respiration) was correlated with the interannual variability in shortwave radiation. Others suggest that along with increases in solar radiation and air temperature, increases in atmospheric CO_2 concentrations have also contributed to accelerated growth of tropical forests in the Amazon basin (Lewis *et al*., 2004a, b).

The goal of this study is to understand whether the observed carbon sequestration in evergreen forest ecosystems of the Amazon basin could be explained by changes in climate alone, or whether other potential drivers, such as elevated CO_2 concentrations must also be considered. To answer this question, we used multiple ecosystem models in combination with multiple climate datasets to simulate and account for the observed trend in the NOAA/AVHRR NDVI data.

Materials and methods

Study area

For our modeling analysis, we selected a study region of the western Amazon extending between 0–10°S and 60–70°W (Fig. 1b). This is the most humid region of the Amazon basin, with mean annual precipitation >2000 mm, and is characterized by smaller rates of deforestation compared with regions in the eastern and southern parts of the Amazon basin (Asner *et al*., 2005), eliminating the need to model deforestation. Also, in this region atmospheric contamination from aerosols caused by biomass burning is small compared with the southeastern Amazon region (Kobayashi & Dye, 2005). Huete *et al*. (2006) observed that the seasonal dynamics of the enhanced vegetation indices (EVI) measured using the MODerate Resolution Imaging Spectroradiometer (MODIS) differ in the eastern and western parts of the Amazon basin. Myneni *et al*. (2007)

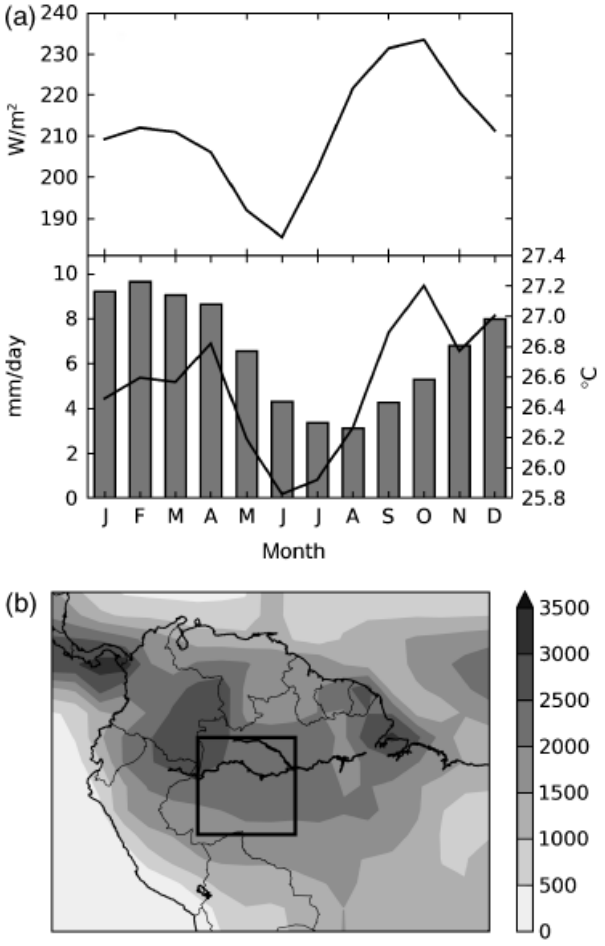

Fig. 1 (a) Mean monthly climatology of the International Satellite Cloud Climatology Project (ISCCP) shortwave radiation (solid line in upper panel), Global Precipitation Climatology Project (GPCP) precipitation (bars in the lower panel), and CRU temperature (solid line in lower panel) within the study region. (b) Map of GPCP mean annual precipitation (1984–2002). The square area surrounded by thick lines is the study area.

also reported a good correlation between the dynamics of satellite observed leaf area index (LAI) and shortwave radiation, rather than precipitation, in the western Amazon. However, the western Amazon has fewer observations of both climate and vegetation compared with the Eastern Amazon. These factors led us to further analyze the carbon balance in the western Amazon using ecosystem models.

Trend analysis of NDVI datasets

We used a 1982–2003 subset of the 8 km resolution NDVI data from the Global Inventory Modeling and Mapping Studies (GIMMS) group. The GIMMS data record is derived from observations collected by the AVHRR instrument onboard the National Oceanic and Atmospheric Administration satellite series (Tucker *et al*., 2005). We used the GIMMS data to analyze the interannual variability in vegetation productivity over the western Amazon in response to changes in climatic variables and atmospheric CO_2 concentrations. The GIMMS NDVI long-term dataset has been georeferenced, atmospherically corrected, and composited to 15-day maximum NDVI values. To correct for the solar zenith angle perturbation, GIMMS used the empirical mode decomposition (EMD) (Pinzón *et al*., 2005). Correction for stratospheric aerosols was made for the two anomalously high aerosol burden periods resulting from emissions from two major volcano eruptions (El Chichon, April 1982 to December 1984; and Mt Pinatubo, June 1991 to December 1994). To further reduce cloud contamination in the study area, we aggregated the GIMMS data into monthly composites by selecting, for each pixel of each month, the maximum value from the 15-day composite GIMMS data.

Intercomparison and trend analysis of climate datasets

We compared several datasets for each climate variable that is required as an input for the ecosystem models. The details for each datasets utilized are listed in Table 1. For regional studies in locations that have a low density of meteorological stations, such as the Amazon basin, it is preferable to use satellite-derived climate

Table 1 Descriptions for each dataset

Parameter	Dataset	Spatial resolution	Time resolution	Time period	Method
Temperature					
	CRU	0.5°	Monthly	1901–2002	i
	UD	0.5°	Monthly	1950–1999	i
	NCEP	ca. 2.5°	6-Hourly	1948–present	m
Precipitation					
	CRU	0.5°	Monthly	1901–2002	i
	GPCP	2.5°	Monthly	1979–present	s,i
	NCEP	ca. 2.5°	6-Hourly	1948–present	m
	UD	0.5°	Monthly	1950–1999	i
Shortwave radiation					
	ISCCP	280 km	Monthly	1983/1987–2004	m
	NCEP	ca. 2.5°	6-Hourly	1948–present	m
Cloud cover					
	ISCCP	280 km	Monthly	1983/1987–2004	m
	NCEP	ca. 2.5°	6-Hourly	1948–present	m

Note that the descriptions are based on the available data. The characters 'i', 's,' and 'm' in the method column indicate the method used to produce the gridded data set: interpolation (i), satellite data (s), and climate model (m).

Published 2009

data to capture the heterogeneity in meteorological observations for the overall region. Some surface-level climate variables, however, are difficult to measure directly from satellite sensors (e.g. incident shortwave radiation), and thus we need to use datasets that are interpolated from ground observations, or modeled datasets as alternatives to satellite-measured climate datasets. The uncertainty in the interpolated datasets depends on the density of meteorological stations in the network, and measurement errors at a single station can have a substantial influence on interpolated estimates for regions with sparse station coverage (Malhi & Wright, 2004). Modeled datasets can also have large systematic errors, and thus the results deduced from the modeled climate datasets (e.g. reanalysis datasets) can be biased (Zhao *et al*., 2006). Therefore, our approach is to first identify common trends in the available datasets, and then compare the trends among datasets to obtain reliable climate trends.

Temperature. We used three temperature datasets: CRU TS 2.1 (Mitchell & Jones, 2005), the Willmott and Matsuura datasets (Legates & Willmott, 1990b) from the University of Delaware (Willmott & Matsuura, 2001), and the NCEP NCAR Reanalysis datasets (Kalnay *et al*., 1996) (hereafter, referred to as CRU, UD, and NCEP, respectively). Both CRU and UD are interpolated datasets derived from data records from ground observation networks using different interpolation algorithms. The NCEP dataset is the product of a global reanalysis that ingests datasets including satellite data, sonde data, aircraft data, surface observations, sea surface temperature data, and other observations. NCEP has many output parameters with varying degrees of accuracy. Kalnay *et al*. (1996) ranked the variables by the extent of model dependency and ranked surface air temperature as the variable on which both models and observations have the most influence, and is therefore the most reliable parameter within the NCEP datasets.

Precipitation. We used the Global Precipitation Climatology Project (GPCP) Version 2 combined precipitation dataset (Adler *et al*., 2003) (hereafter, refer to as GPCP), as well as precipitation data from the CRU, UD (Legates & Willmott, 1990a), and NCEP datasets. GPCP combines several satellite and gauge network datasets to calculate a monthly gridded precipitation data product. NCEP does not ingest surface observations of precipitation from gauges, and thus was categorized as a model-derived variable by Kalnay *et al*. (1996), which means that it is less reliable relative to the other NCEP parameters. Both CRU and UD precipitation data are interpolated (as with temperature) from ground-based observation records.

Shortwave radiation and cloud cover. Currently, there is no method to directly measure the downward shortwave radiation fluxes at the land surface level using satellites. There are, however, two model-derived datasets available for long-term analysis: the International Satellite Cloud Climatology Project (ISCCP) datasets (ISCCP-FD) (Zhang *et al*., 2004), and the NCEP shortwave radiation dataset. ISCCP provides incident shortwave radiation flux data at the surface level from 1984 to present. ISCCP shortwave radiation data are calculated using the radiative transfer code from the GISS Global Circulation Model (GCM), which ingests multiple global climate datasets. The NCEP downward shortwave radiation dataset is also categorized by Kalnay *et al*. (1996) as a model-derived variable, similarly to NCEP precipitation. The comparison, reviews, and validation for the ISCCP and NCEP datasets were thoroughly addressed by Hicke (2005).

We also used cloud cover datasets from ISCCP and NCEP in place of shortwave radiation as an input for the LPJ ecosystem model. As with the downward shortwave radiation flux, cloud cover in the NCEP dataset is categorized as a model-derived variable. We did not use cloud cover data from CRU, as none of the ground stations used for interpolation were located inside the study region. Furthermore, the CRU cloud cover data are derived from cloud cover observations collected from 1971 to 1995, and sunshine duration measurements from 1996 to 2001, with no overlapping period between the two inputs (Mitchell & Jones, 2005).

Since the detection of trends in cloud cover from the ISCCP dataset is prone to artifacts at the edges of the field of view of the satellites from which these observations are derived (Evan *et al*., 2007), we used the Earth Radiation Budget Experiment (ERBE) S-10N NF Edition 3 dataset (Barkstrom, 1984) and Clouds and the Earth's Radiant Energy System (CERES) ES-4 datasets (Wielicki *et al*., 1996) to validate the results of the trend analysis of cloud cover data from ISCCP and NCEP datasets. The ERBE S-10N NF Edition 3 datasets (hereafter, referred to ERBE) includes top-of-the-atmosphere (TOA) reflected shortwave radiation, albedo, and total irradiance data measured by the nonscanner instrument carried by the Earth Radiation Budget Satellite (ERBS) spacecraft, and are available from 1984 to 1999. We calculated monthly downward shortwave radiation from the 5° grid of ERBE data measured by the middle field-of-view (MFOV) detector. CERES is the project that succeeded ERBE in measuring the global radiation budget. CERES ES-4 datasets represent one of the radiation flux products

Table 2 Comparison of components of the three models used in this study (CASA, Biome-BGC, and LPJ)

	CASA	Biome-BGC	LPJ
Model type	Diagnostic model	Prognostic model	Prognostic model with dynamic vegetation
Climate input	Air temperature Precipitation Shortwave radiation	Maximum air temperature Minimum air temperature Precipitation Shortwave radiation VPD	Air temperature Precipitation Cloud cover Wet day
Photosynthesis model	Monteith-type LUE model (Monteith, 1972)	Farquhar biochemical model (Farquhar *et al*., 1980) with Jarvis-type empirical stomatal conductance model (Jarvis, 1976)	Combination of biochemical model (Haxeltine & Prentice, 1996) based on Farquhar *et al*. (1980) and Ball-type empirical stomatal conductance model (Ball *et al*., 1987)
ε_{max} or V_{cmax}*	Predefined biome-specific ε_{max}	V_{cmax} from leaf nitrogen and Rubisco activity	V_{cmax} from optimal nitrogen allocation with canopy (Haxeltine & Prentice, 1996)
Parameters constraining photosynthesis	Shortwave radiation CO_2 concentration (optional) Air temperature Soil water content FPAR	Shortwave radiation CO_2 concentration Soil water content Air temperature VPD LAI Leaf nitrogen content	Shortwave radiation CO_2 concentration Soil water content Air temperature FPAR LAI
Evapotranspiration model	De Marsily (1986)	Penman–Monteith equation with Jarvis stomatal conductance model (Jarvis, 1976)	Equilibrium evapotranspiration restricted by water availability
Autotrophic respiration model	Not calculated	Maintenance respiration calculated by Q_{10} model regulated by the nitrogen contents. Growth respiration of prescribed ratio of carbon storage rate	Maintenance respiration calculated by Q_{10} model accounting for acclimation with prescribed coefficient for each plant functional type. Growth respiration of 25% of the residual of GPP subtracted from maintenance respiration
Reference	Potter *et al*. (1993)	Thornton *et al*. (2002)	Sitch *et al*. (2003) and Gerten *et al*. (2004)

*ε_{max} is the canopy-level maximum light use efficiency. V_{cmax} is the maximum carboxylation rate of Rubisco.
LAI, Leaf Area Index; VPD, Vapor Pressure Deficit; FPAR, fraction of absorbed photosynthetically active radiation by vegetation.

derived from CERES instruments carried by TRMM, Terra, and Aqua spacecraft, and were calculated using the same algorithm used for ERBE data. We averaged the monthly CERES data from the products observed by the available sensors (Terra-FM1, Terra-FM2, Aqua-FM3, and Aqua-FM4).

Ecosystem model experiments

NPP variations are generally representative of corresponding variations in NDVI (Schloss *et al*., 1999). We calculate NPP from three ecosystem carbon models: CASA (version 2003.04.29) (Potter *et al*., 1993), Biome-BGC (version 4.2) (Thornton *et al*., 2002), and LPJ (version 1.2) (Sitch *et al*., 2003; Gerten *et al*., 2004). Detailed features of the three models are summarized in Table 2.

CASA is a diagnostic model that requires NDVI data as an input, from which LAI and fraction of absorbed photosynthetically active radiation (PAR) by vegetation (FPAR) are estimated using empirical equations. In CASA, NPP is calculated as the product of maximum Light Use Efficiency (ε_{max}), PAR, FPAR, and climate-driven regulation factors, which are functions of air temperature and soil water content. Optionally, CASA can use CO_2 concentration data to simulate the CO_2 fertilization effect on NPP. However, since the modeling of the CO_2 fertilization effect in CASA is very simple,

Published 2009

with photosynthesis linearly increasing with CO_2 concentrations, we did not use this feature of CASA in our study.

Biome-BGC is a prognostic biogeochemical model driven by climate data for the prescribed land cover. Biome-BGC uses the Farquhar biochemical photosynthesis model (Farquhar *et al*., 1980) to calculate GPP, and estimates NPP as the remainder of GPP subtracted from autotrophic respiration, which is a function of temperature and biomass. Stomatal conductance in Biome-BGC is modeled using a Jarvis-type model (Jarvis, 1976) as the product of predefined maximum stomatal conductance and climate regulation factors [shortwave radiation, air temperature, soil water potential, and vapor pressure deficit (VPD)]. Globally applicable models sometimes require tuning for regional applications (Thornton *et al*., 2002). In this study, the main model and ecophysiological parameters of Biome-BGC were from Ichii *et al*. (2007), which adjusted the submodels and parameters to match the Tapajós flux data (Saleska *et al*., 2003). Also, to match the seasonal variation in GPP measured at the Tapajós flux site, we added a submodel of seasonal variations in percent of leaf nitrogen in Rubisco, following Ichii *et al*. (2007). A combined satellite and model study (Ichii *et al*., 2007) and an *in situ* plot study (Nepstad *et al*., 1994) both suggested that very deep root systems (deeper than 5 m) exist in the Amazon tropical forests. Thus, we set the rooting depth at 5 m (vs. the default value of 1 m).

LPJ is also a prognostic model, but includes a dynamic biogeography submodel, which determines the land cover implicitly from climate data. The plant functional types in the Amazon were mostly categorized as tropical broad-leaved evergreen by the LPJ dynamic biogeography submodel. As with Biome-BGC, LPJ uses the Farquhar biochemical photosynthesis model (Haxeltine & Prentice, 1996), and subtracts autotrophic respiration from GPP. Autotrophic respiration is controlled by air temperature. Stomatal conductance in LPJ is estimated from a Ball-type conductance model (Ball *et al*., 1987). We did not adjust any of the default parameters.

To obtain the initial allocation of carbon in an ecosystem (i.e. the allocation to leaves, stems, roots, soil, etc.), carbon ecosystem process models require a spin-up period, during which the model runs until it reaches an equilibrium state for the desired climate conditions. We used climate data from the run period (i.e. 1984–2002, except for the experiments that used UD data from 1984 to 1999) for the spin-up for each model. Using averages from the climate data for the entire study period to spin-up the models would have led to a value of 0 for the total net ecosystem exchange (NEE) from 1984 to 2002.

To identify the climate variable(s) driving the observed trend in vegetation dynamics over the western Amazon forests, we followed the methodology adopted by Ichii *et al*. (2005), in which the ecosystem model runs are driven by changing a single climate variable while keeping the other climate variables fixed. The climate variables that remain fixed during the modeling experiments are calculated as monthly averages for 1984–2002 from the selected datasets, including CRU for temperature, GPCP for precipitation, and ISCCP for radiation and cloud cover. CRU temperature data were selected because they are derived from interpolation of at least 20 stations in the study region from 1984 to 2002, and therefore are deemed to reliably represent the monthly temperature climatology for the western Amazon. An intercomparison study of global precipitation datasets indicated that the latitudinal average of GPCP showed the most reasonable profile (with the least number of outliers) relative to the other datasets (Fekete *et al*., 2004). Shortwave radiation and cloud cover were selected from the ISCCP dataset, as Hicke (2005) showed these data agreed more closely with observations than NCEP radiation. Figure 1a shows the seasonal climatology of the study region from CRU temperature, GPCP precipitation, and ISCCP shortwave radiation.

For Biome-BGC, which uses daily rather than monthly climate inputs, we also calculated daily anomalies. The daily anomalies were calculated as deviations from the monthly average of temperature, precipitation and solar radiation from the NCEP dataset, which is the only dataset that provides daily values. For LPJ, we used the weather generator (Gerten *et al*., 2004) to derive daily climate data from the monthly climate inputs.

The observed trends in climate variables are sometimes only detectable during specific months, and analysis of yearly averages can be insufficient to understand the phenomenon of climate change. For example, Chagnon & Bras (2005) found a shift in the seasonality of precipitation from a gauge record that spanned 75 years. Since the responses of models to climate change can vary depending on the season, for all the modeling experiments we calculated both annual and monthly trends in NPP.

To assess the influence of elevated CO_2 concentration on the modeled NPP, we used the CO_2 concentration data observed at Mauna Loa, Hawaii, as no continuous data record was found at a more proximate location for our study period. While there are almost certainly differences in the absolute CO_2 concentrations between Mauna Loa and the Amazon basin, the relative change in concentrations over time both at Mauna Loa and in the Amazon basin is expected to be consistent. Thus, the results of the simulations using the Mauna Loa CO_2

Published 2009

concentration should be deemed appropriate for the purpose of our study.

Tests for trend analysis

To detect trends in climate and carbon cycling, we used the Mann–Kendall trend test (Kendall, 1938). Compared with the linear regression trend test, the Mann–Kendall trend test has the following advantages. First, the Mann–Kendall trend test does not require the assumption of normality in the variance. Perturbation events to the climate system such as the Mt. Pinatubo eruption or ENSO events could invalidate the normal distribution assumption. Second, because the Mann–Kendall trend test relies on rank-based statistics, an anomalous outlier on the edge of a time-series data record does not have a strong effect on the test result.

The slope of the trends was calculated from the Kendall–Theil robust line (Helsel & Hirsch, 1992). The Kendall–Theil robust line is defined as the line whose slope is the median of all possible pair-wise slopes of the data, and is on the median of both variables. Hence, the Kendall–Theil robust line is also relatively insensitive to outliers on the edge.

Results and discussion

NDVI trend

The regional average of the annual mean NDVI for the study region shows a significant positive trend (P-value < 0.05) (Fig. 2a). The large drop in annual mean NDVI observed in 1991 was due to the eruption of Mt. Pinatubo. A comparison of monthly average NDVI between two different periods (1982–1990 and 1993–2003) indicates that the positive trend in annual mean NDVI was due mainly to decadal increases in NDVI between the months of August and December, with November and December showing especially strong significant positive trends (P-value < 0.05) (Fig. 2b).

The biggest limitation of optical remote sensing analysis in the humid tropics is cloud contamination, especially for data with moderately coarse resolution such as AVHRR. Although we made monthly composite NDVI data to minimize the cloud contamination effect, residual contamination may still be present and could result in artificial trends. The saturation of NDVI over dense forests also makes trend analysis difficult. For example, during the months of June and July, monthly NDVI values are close to 0.8, suggesting that observed increases in NDVI are difficult to interpret (Fig. 2b). However, a consistent shift in seasonal cycle is apparent between the two decades (Fig. 2b), with strong increases in NDVI during the dry season.

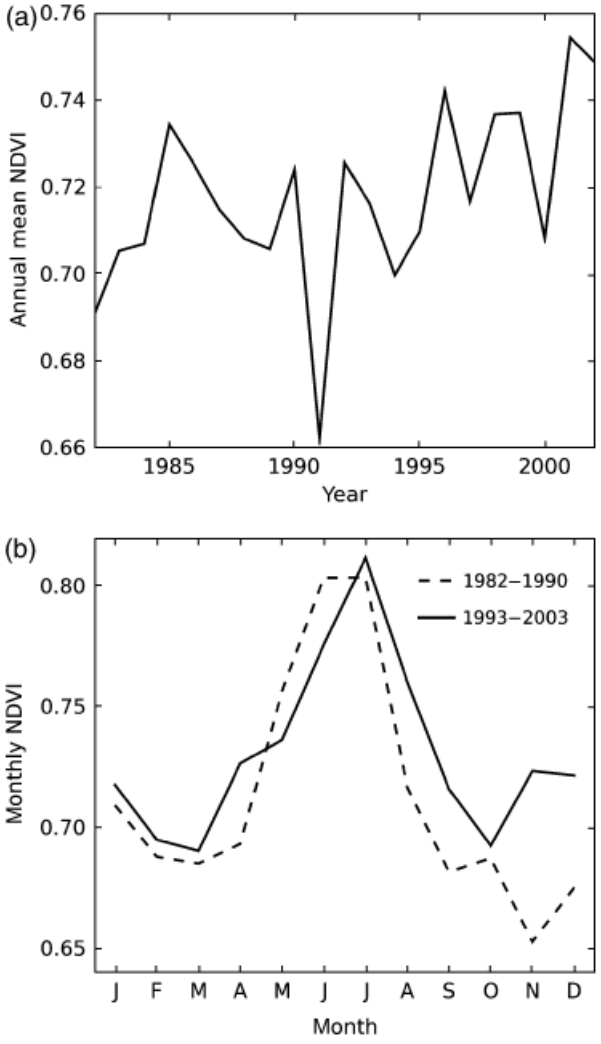

Fig. 2 (a) Interannual variability in the yearly mean Normalized Difference Vegetation Index (NDVI) for the study region from 1982 to 2003. (b) Monthly average of NDVI from 1982 to 1990 (broken line) and from 1993 to 2003 (solid line). Values at each time step are the average value of all grid cells inside the study region.

Comparison of climate datasets

Temperature trends. Positive trends in temperature are present in the interpolated datasets (CRU and UD) but not in NCEP (Fig. 3). Victoria *et al*. (1998) also reported a positive trend result in the Amazon basin since the 1970s, and found that temperature in the Amazon basin has increased at a rate similar to the overall warming rate for the southern hemisphere. The average monthly temperature values for the interpolated datasets (CRU and UD) are very close, but higher than NCEP by approximately 1.5 °C. For the study period from 1984 to 2002, only CRU showed a statistically meaningful positive trend of $0.05^{\circ}\,yr^{-1}$

Published 2009

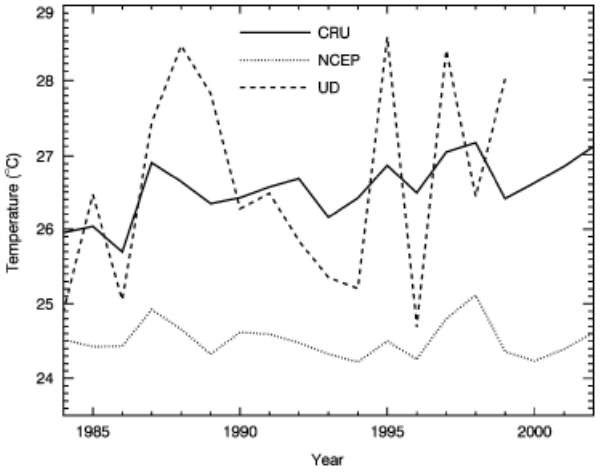

Fig. 3 Interannual variability in the yearly average temperature for each climate dataset from 1984 to 2002 (CRU, NCEP, and UD). Values at each time step are the average value of all grid cells inside the study region.

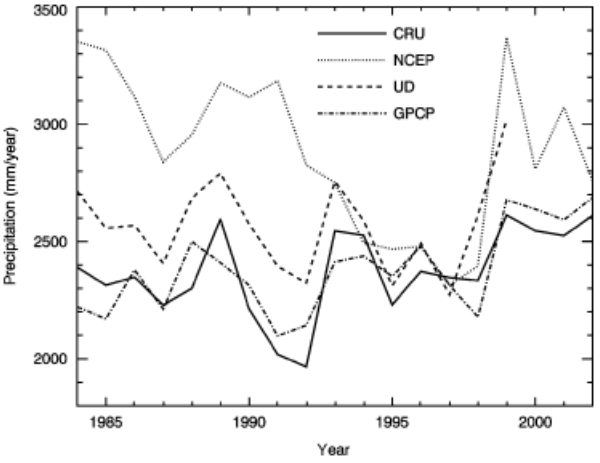

Fig. 4 Interannual variability in the yearly average precipitation for each climate dataset 1984–2002 [CRU, NCEP, UD, and Global Precipitation Climatology Project (GPCP)]. Values at each time step are the average value of all grid cells inside the study region.

Table 3 The trend in the yearly average of each climate dataset

Parameter	Dataset	Trend
Temperature (deg. yr^{-1})	CRU	0.05*
	UD	0.04
	NCEP	−0.01
Precipitation (mm day^{-1} yr^{-1})	CRU	0.03
	GPCP	0.06*
	NCEP	−0.10*
	UD	−0.02
Shortwave radiation (W m^{-2} yr^{-1})	ISCCP	0.48*
	NCEP	0.48*
Cloud cover (% yr^{-1})	ISCCP	−0.36*
	NCEP	−0.13

*Indicates that the *P*-value of the Mann–Kendall trend test was <0.05.

(Table 3). Malhi & Wright (2004) also found a positive temperature trend in the CRU dataset for the period 1976–1998 in the central Amazon, which includes our study region.

Precipitation trends. The precipitation trend for the study period (1984–2002) was significantly positive in GPCP (0.06 mm day^{-1} yr^{-1}), but no significant trend was detected in the CRU and UD datasets (Table 3). A significant negative trend was detected in NCEP precipitation data (−0.10 mm day^{-1} yr^{-1}). NCEP data clearly deviate from the other three datasets (CRU, UD, and GPCP) until 1992 (Fig. 4). Such a discrepancy in NCEP precipitation data was also reported in Marengo *et al*. (2008).

There are many publications that discuss trends in precipitation in the Amazon basin. For example, the northern Amazon basin has shown a negative trend in precipitation since 1950, but a positive trend has been observed in the southern Amazon basin (Marengo, 2004). Malhi & Wright (2004) investigated the CRU precipitation dataset for the existence of trends in rainfall in the pan-tropics, but found no significant trend in the Amazon from 1960 to 1998. Results of those publications are highly dependent on the datasets, study period, and study region used, and are complicated by the heterogeneity of precipitation in the Amazon.

Shortwave radiation and cloud cover trend. For the study period, ISCCP and NCEP showed similar significant positive trends (0.48 W m^{-2} yr^{-1}) in shortwave radiation (Table 3), although the magnitudes of the monthly averages are quite different from each other (Fig. 5a). Consistent with the increasing trends in shortwave radiation, both ISCCP and NCEP cloud cover data show significantly negative trends (ISCCP: −0.36% yr^{-1}; NCEP: −0.13% yr^{-1}). Cloud cover in the two datasets also has very different monthly average magnitudes (Fig. 6).

The ERBE and CERES data also showed increasing trends in downward shortwave radiation in the 1980s and 1990s (Fig. 5b). ERBE and CERES data represent the radiation flux at the Top of the Atmosphere (TOA) rather than at the surface. However, since the amount of shortwave radiation absorbed by the atmosphere is small compared with the amount absorbed by the land surface, the positive trends found in the ERBE and

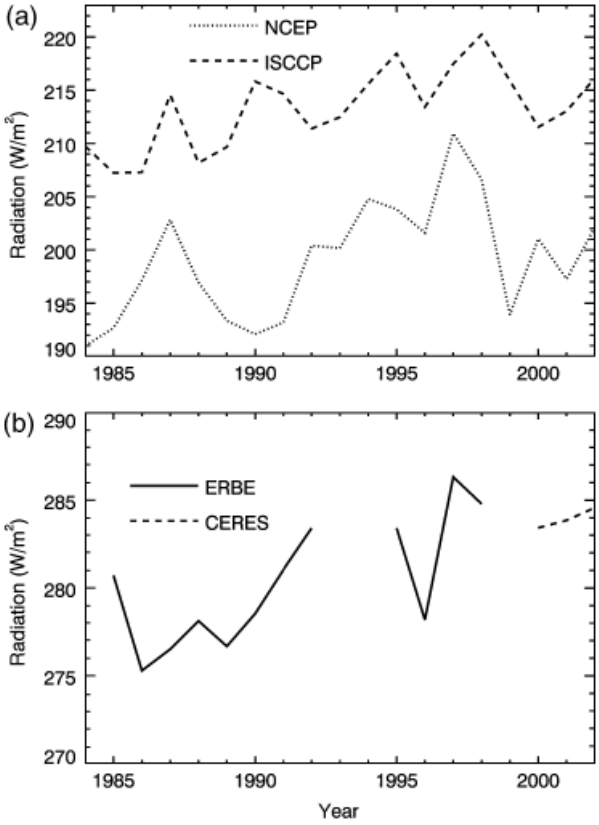

Fig. 5 (a) Interannual variability in the yearly average shortwave radiation at the surface for each climate dataset from 1984 to 2002 [NCEP and International Satellite Cloud Climatology Project (ISCCP]. (b) Interannual variability in the yearly average downward shortwave radiation at the top of the atmosphere from Earth Radiation Budget Experiment (ERBE) (solid line) and Clouds and the Earth's Radiant Energy System (CERES) (broken line). Values at each time step are the average value of all grid cells inside the study region.

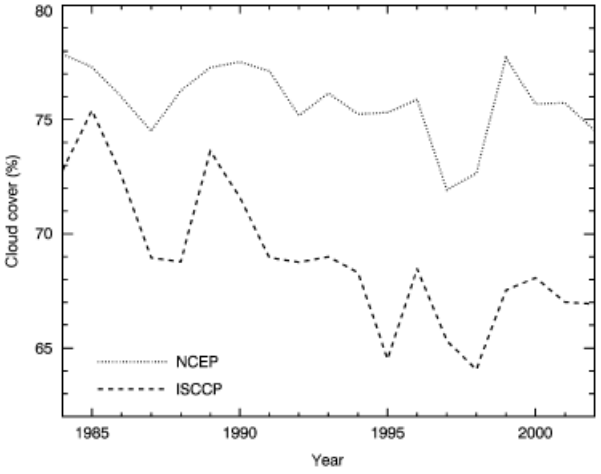

Fig. 6 Interannual variability in the yearly average cloud cover for each climate dataset from 1984 to 2002 [NCEP and International Satellite Cloud Climatology Project (ISCCP)]. Values at each time step are the average value of all grid cells inside the study region.

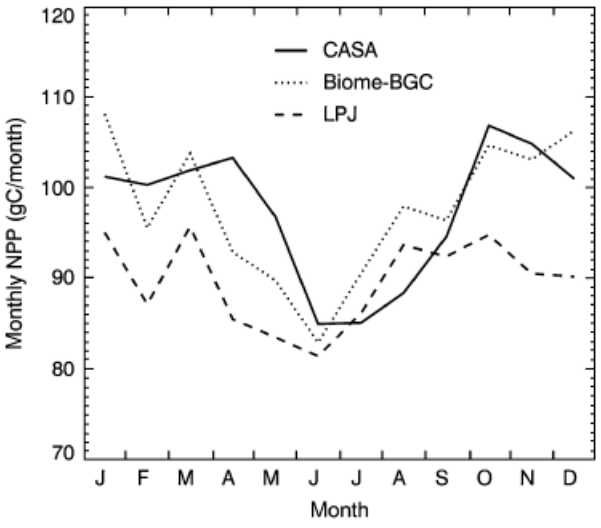

Fig. 7 Monthly mean net primary production (NPP) for each model (CASA, Biome-BGC, and LPJ) from 1984 to 2002. Values shown are the average value of all grid cells inside the study region.

CERES datasets also imply an increase in absorbed shortwave radiation at the surface over the two decades analyzed in this study.

Globally, while solar dimming has been observed through the 1980s (Stanhill & Cohen, 2001), solar radiation has been shown to be increasing since the late 1980s (Wild *et al*., 2005). In the tropics, the increasing trend in incoming shortwave radiation was reported from satellite observations and attributed to decadal time-scale strengthening of the tropical Hadley and Walker circulations (Chen *et al*., 2002; Wielicki *et al*., 2002). In addition to wide scale climate change, changes in the regional-scale hydrologic cycles (shallow cumulus cloud and precipitation patterns) were reported as a result of deforestation (Chagnon *et al*., 2004; Chagnon & Bras, 2005). These observations strengthen the conclusion that the shortwave radiation budget for the Amazon basin is changing, as a consequence of climate change and/or land use change.

Modeling experiments

Seasonal variation in simulated monthly NPP. For all three models, Fig. 7 shows that the minimum mean monthly NPP occurs in July, as does the minimum in solar radiation (Fig. 1a). On the other hand, the month in which the peak in mean monthly NPP occurs differs among the three models, with the peak occurring in October, January, and March for CASA, Biome-BGC,

Published 2009

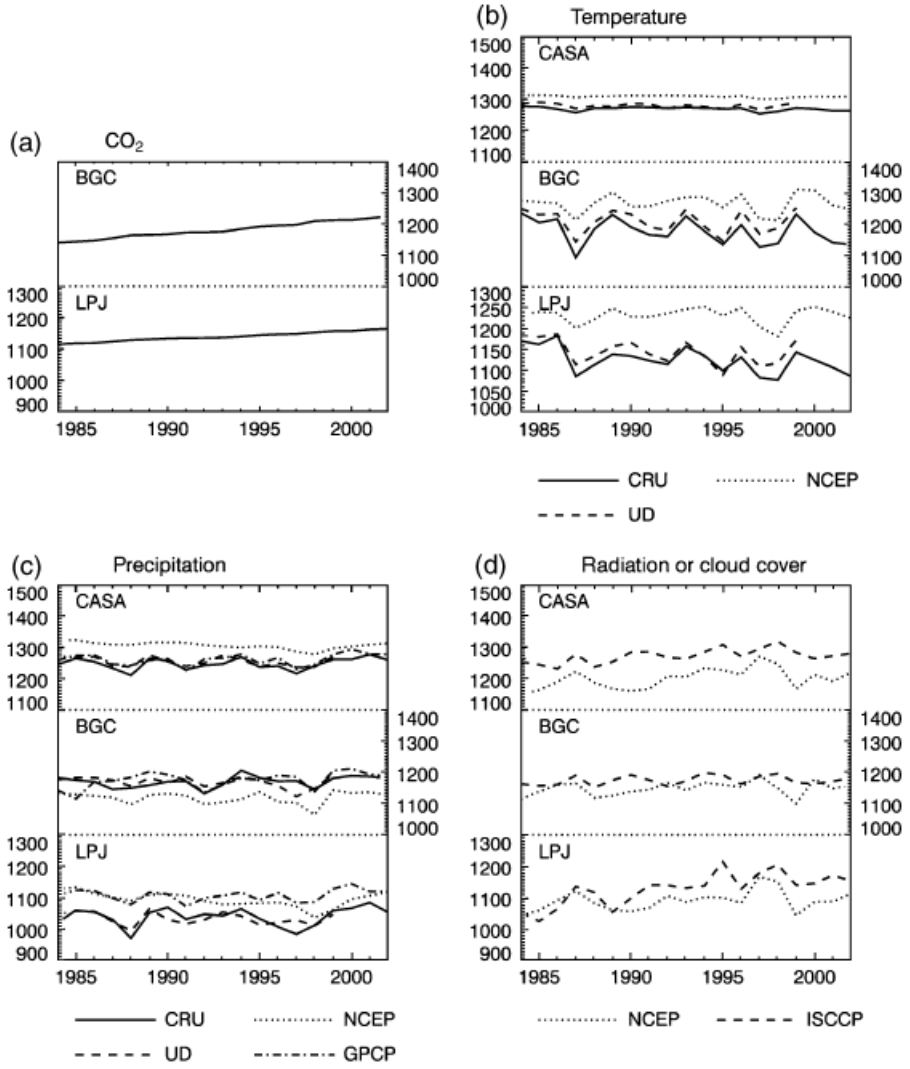

Fig. 8 Net primary production (NPP) time series for each model experiment for (a) changing CO_2 concentrations, (b) changing temperature, (c) changing precipitation, and (d) changing shortwave radiation or cloud cover. The solid, broken, dashed, and dash-dot lines represent the different datasets listed under each panel. The unit for the vertical axes is $g\,C\,m^{-2}\,yr^{-1}$. Note that we did not implement the CO_2 experiment for CASA because of its simplicity, and thus there is no result shown for CASA in (a), the changing CO_2 experiment panel. Values at each time step are the average value of all grid cells inside the study region.

and LPJ, respectively. Overall, the seasonal cycle of NPP from all three models peaks in the dry season, with minimum values occurring during the wet season. This pattern indicates that water availability did not limit monthly NPP during the dry season, but shortwave radiation did limit monthly average NPP during the wet season. Thus, shortwave radiation appears to be the primary driver of seasonal patterns in NPP. These simulated seasonal cycles are similar to the observed patterns in GPP at the Tapajós site (Hutyra *et al*., 2007). Ichii *et al*. (2007) explained nonwater limitations using Biome-BGC with a deep rooting soil depth ($>5\,m$). Other than seasonal cycles of shortwave radiation, leaf production in the dry season (Hutyra *et al*., 2007) and increases in diffusive radiation caused by aerosols resulting from biomass burning (Oliveira *et al*., 2007) should also contribute to high monthly NPP in the dry season, but none of the models used in this study accounted for them.

Elevated CO_2 concentration experiments. The modeling experiments to examine the effect of increased CO_2 concentrations using both Biome-BGC and LPJ show a monotonous positive trend in NPP that corresponds with the monotonous increase in atmospheric CO_2 concentrations (Fig. 8a). The rate of increase in annual NPP is $4.66\,(g\,C\,m^{-2}\,yr^{-1})\,yr^{-1}$ for Biome-BGC and $2.67\,(g\,C\,m^{-2}\,yr^{-1})\,yr^{-1}$ for LPJ, and is statistically

Table 4 The slope of the trend [$(g\,C\,m^{-2}\,yr^{-1})\,yr^{-1}$] in the yearly NPP calculated from each ecosystem model and each climate dataset

	Data set	CASA	BGC	LPJ
CO_2			4.66*	2.67*
Temperature				
	CRU	−0.54*	−4.01	−3.49*
	NCEP	−0.24*	−0.17	0.30
	UD	−0.47	−1.18	−2.75
Precipitation				
	CRU	0.59	0.99	0.88
	NCEP	−1.20*	0.10	−2.81*
	UD	0.98	1.93*	0.59
	GPCP	−0.74	−1.12	−1.30
Shortwave radiation or cloud cover				
	NCEP	3.17*	1.42	2.34
	ISCCP	2.18*	0.71	6.35*

*Indicates that the *P*-value of the Mann–Kendall trend test was <0.05.

significant per the Mann–Kendall trend test (Table 4). Note that the CO_2 concentration experiment was not implemented for CASA, although given the linear relationship between CO_2 concentrations and photosynthesis in the model, one would expect the results from CASA to show a linear increase in NPP that tracks the increase in the CO_2 concentration data.

Temperature sensitivity experiments. All models simulate higher NPP when using temperature from NCEP rather than from CRU and UD (Fig. 8b), primarily because the lower air temperature in the NCEP data (Fig. 3) reduced the amount of autotrophic respiration. Interannual fluctuations in autotrophic respiration are a function of air temperature and drive the interannual variation in NPP simulated from Biome-BGC and LPJ (Table 2). In contrast, CASA calculates NPP directly, as opposed to via GPP, resulting in smaller interannual fluctuations in NPP than for the Biome-BGC and LPJ models. In addition, the air temperature in the study region during the period analyzed displayed small interannual and seasonal variability, remaining close to the optimum temperature for photosynthesis defined in the CASA model (CASA defines the optimum temperature for photosynthesis as the temperature recorded when NDVI reaches the annual maximum). The higher variability of temperature data in the UD dataset (Fig. 3) does not have a large impact on NPP variability for all three models, because of reduced sensitivity to temperature in the models. The variability in NPP is similar in each model for all three of the temperature datasets used in the modeling analysis.

Precipitation sensitivity experiments. The year-to-year variations in NPP as a function of the precipitation dataset are dependent on the model used, with the variations in NPP simulated from LPJ being higher than those from CASA and Biome-BGC (Fig. 8c). Within each model, the interannual variation in NPP is very similar for all of the precipitation datasets, except for NCEP, which was an outlier in the CASA and Biome-BGC simulations. The trends are very different among the models and climate datasets (Table 4). Significant negative trends in annual NPP were found when using the NCEP-CASA [$-1.20\,(g\,C\,m^{-2}\,yr^{-1})\,yr^{-1}$] and NCEP-LPJ [$-2.81\,(g\,C\,m^{-2}\,yr^{-1})\,y^{-1}$], which responded to the decreasing trend observed in the NCEP precipitation data ($-0.10\,mm\,day^{-1}\,yr^{-1}$). On the other hand, the NPP modeled by Biome-BGC showed a significant positive trend only when using the UD precipitation dataset [$1.93\,(g\,C\,m^{-2}\,yr^{-1})\,yr^{-1}$].

Shortwave radiation or cloud cover experiments. All modeling experiments showed positive trends in annual NPP driven by increases in shortwave radiation and/or declines in cloud cover (Table 4). A significant positive trend in NPP was calculated in the simulations from NCEP-CASA [$3.17\,(g\,C\,m^{-2}\,yr^{-1})\,yr^{-1}$], ISCCP-CASA [$2.18\,(g\,C\,m^{-2}\,yr^{-1})\,yr^{-1}$], and ISCCP-LPJ [$6.35\,(g\,C\,m^{-2}\,yr^{-1})\,yr^{-1}$] (Fig. 8d). Biome-BGC was less sensitive to shortwave radiation than CASA and LPJ. Therefore, the increasing trend in shortwave radiation was the only climate factor which clearly and consistently drove the increasing trend in annual NPP.

Monthly trends of model outputs and climate datasets

The trends in monthly NPP, as calculated by the three models, are summarized in Fig. 9. The increases in atmospheric CO_2 concentration recorded over the study period had a positive impact on the monthly NPP trend for all seasons in both Biome-BGC and LPJ (Fig. 9a). Thus, the increasing trend in CO_2 concentrations cannot explain the positive trends in NDVI observed in specific months.

The temperature experiments with CRU data showed the strongest temperature-related impact on NPP for all three models. All the temperature experiments showed small negative trends for the months from July to October (Fig. 9b). So, none of temperature experiments can explain the positive trend in NDVI observed during these months.

Similar to the precipitation effects on annual NPP (Fig. 8), the impacts of precipitation on the monthly NPP trends varied considerably, depending on the input dataset, even when using the same model for the simulation (Fig. 9c). Among these experiments, only the Biome-BGC experiment driven by UD precipitation

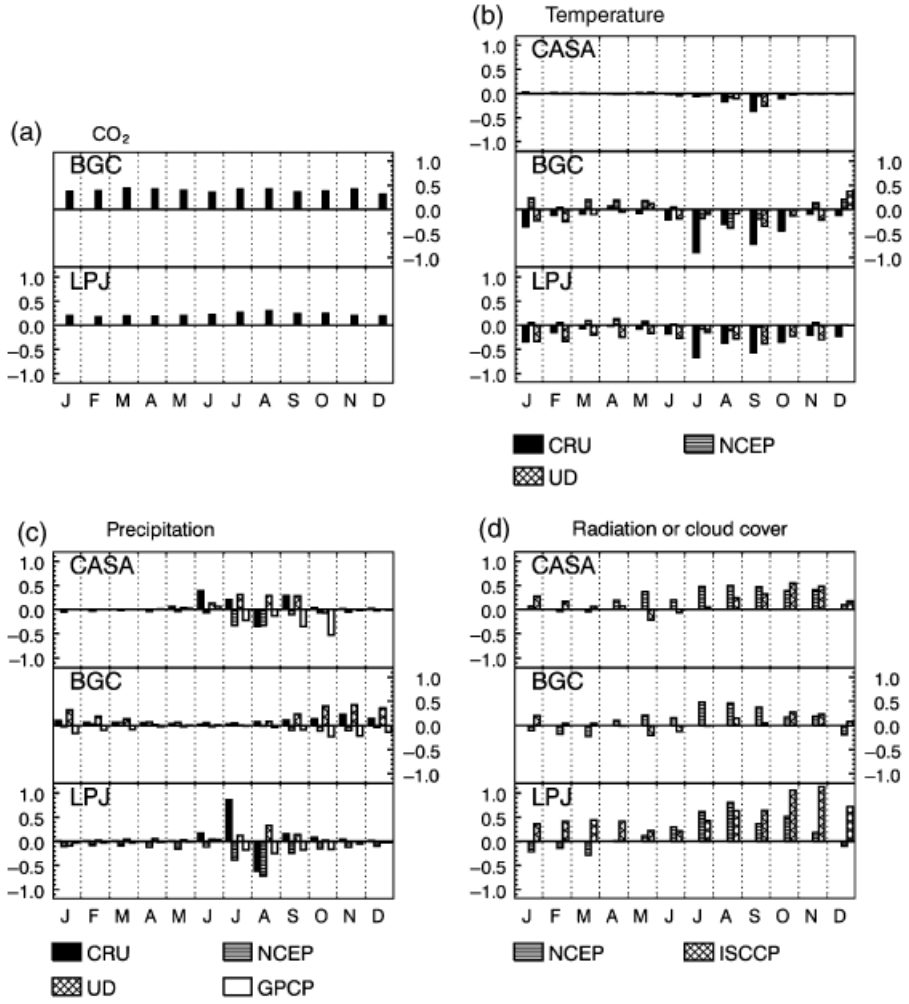

Fig. 9 Trends in monthly net primary production (NPP) (in $g\,C\,m^{-2}\,month^{-1}\,yr^{-1}$) for the three models (CASA, Biome-BGC, and LPJ) for the period from 1984 to 2002 for each climate variable [(a) CO_2, (b) temperature, (c) precipitation, (d) shortwave radiation or cloud cover]. The names of the dataset used in each experiment are listed under each panel. Values shown are the average value of all grid cells inside the study region.

data, which showed a weak positive trend in monthly NPP from September to February, could be a candidate to explain the observed increases in NDVI.

The radiation/cloud cover experiments simulated strong positive trends in NPP from July to December with CASA and LPJ driven by the NCEP and ISCCP datasets, and with Biome-BGC driven by the NCEP (Fig. 9d). These results suggest that the increasing trend in shortwave radiation is the most likely driver of the positive NDVI trends observed from August to December, as opposed to changes in CO_2 concentrations, temperature, or precipitation.

Sensitivity test for model response to changes in climate factors

Increasing shortwave radiation from NCEP and ISCCP caused an increase in NPP from July to December in the CASA and LPJ simulations, while only the NCEP shortwave radiation data resulted in a positive trend in the Biome-BGC simulations (Fig. 9d). Based on the Biome-BGC simulations, the UD precipitation data could also explain the positive NDVI trends from October to December (Fig. 9c). These differences in the effects of climate on simulated NPP originated from the varying model sensitivities to the climate factors.

The responses to variations in temperature were very different among models (Fig. 10a). The NPP simulated by CASA peaked around the optimum temperature for photosynthesis of 26 °C. The NPP modeled by Biome-BGC also peaked at 26 °C, due to the difference in the rate of increase in photosynthesis vs. autotrophic respiration as a function of higher temperatures. LPJ, in contrast, showed a monotonous decrease in response to increasing temperature because photosynthesis in-

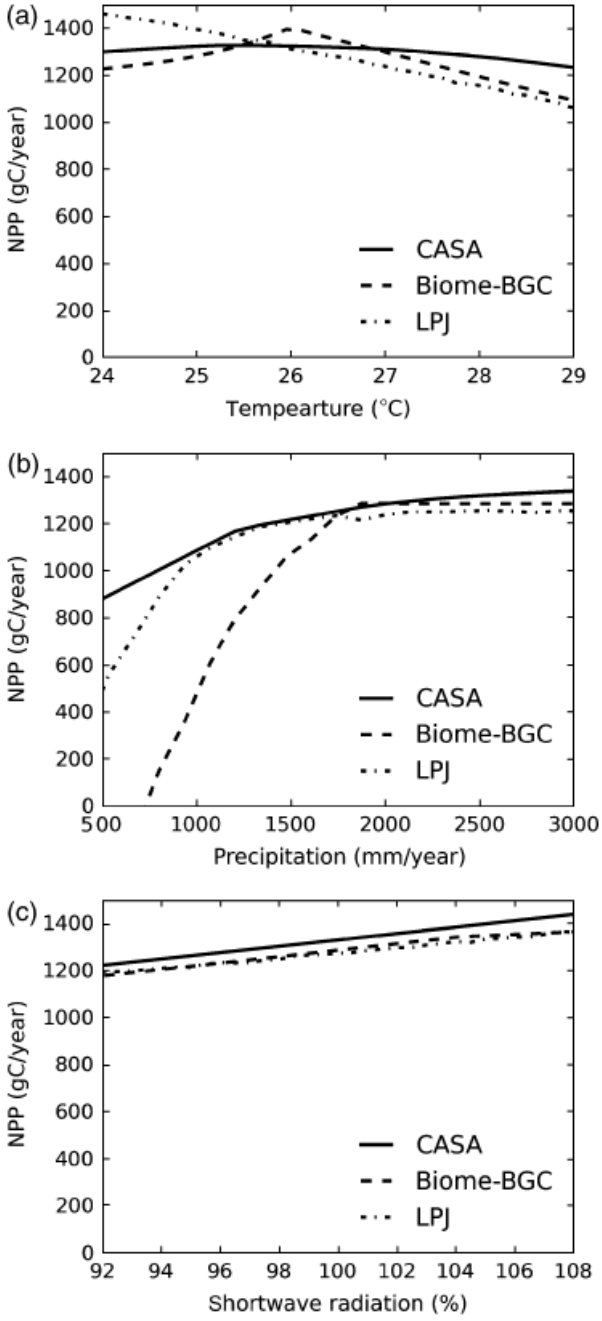

Fig. 10 Model sensitivity test of net primary production (NPP) for three models (CASA, Biome-BGC, and LPJ) by changing climate, (a) temperature, (b) precipitation, and (c) shortwave radiation. Values shown are the average value of all grid cells inside the study region.

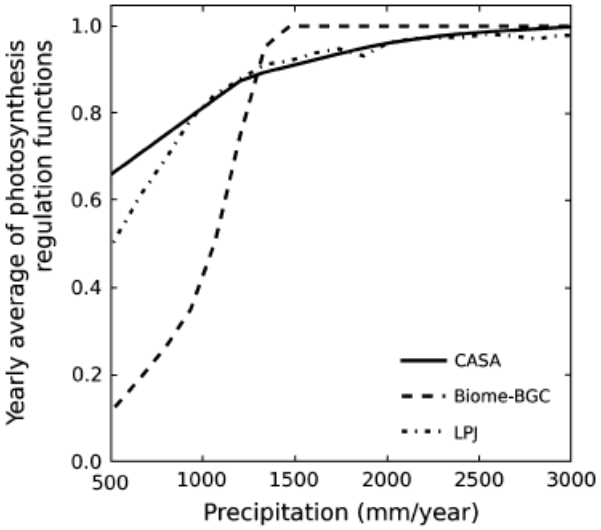

Fig. 11 Sensitivity of yearly average of photosynthesis regulation functions from three models (CASA, Biome-BGC, and LPJ). Values shown are the average value of all grid cells inside the study region.

creased more slowly compared with autotrophic respiration.

The models were most sensitive to variations in precipitation (Fig. 10b). CASA NPP decreased gradually in response to lower precipitation. On the other hand, Biome-BGC and LPJ showed steep drops below a critical level of annual precipitation, with Biome-BGC dropping at a precipitation level of 1800 mm or less, and LPJ dropping at a level of 1000 mm or less, with the difference due to the photosynthesis submodels within these two models. All of the models have multiplier functions in their photosynthesis submodels that limit photosynthesis in response to lack of water, which is represented by soil moisture deficit. Figure 11 shows the dependency of such photosynthesis regulation functions on soil moisture levels, which in turn are driven by precipitation levels such as those shown in Fig. 10b. As compared with NPP, the photosynthesis regulation function in Biome-BGC is more sensitive to precipitation, and regulates photosynthesis strongly when annual precipitation is below a critical threshold of 1300 mm. This critical annual precipitation threshold regulating photosynthesis depends on the soil parameterization, indicating that that proper parameterization of the rooting depth defined in Biome-BGC is very important (Ichii *et al*., 2005). The average yearly amount of evapotranspiration simulated for the study region was 1486 mm in CASA, 2173 mm in Biome-BGC, and 823 mm in LPJ, when using CRU temperature, GPCP precipitation, and ISCCP shortwave radiation. The average yearly precipitation in the study region was 2369 mm in GPCP. Since observations at Manaus indicate that 54% of rainfall (1279 mm) was lost by evapotranspiration from September 1995 to August 1996 (Malhi *et al*., 2002), it is likely that the evapotranspiration calculated by Biome-BGC was too high, suggesting that our Biome-BGC experiments adjusted for Tapajós flux data are still too sensitive to precipitation for the

western Amazon basin, resulting in a higher critical precipitation point for Biome-BGC compared with the other models. Gerten *et al.* (2004) showed good agreement between observed and LPJ-modeled annual runoff, but the seasonal variation of runoff from LPJ was not consistent with the observed data. The peak in LPJ-modeled runoff was in the wet season, while the observed peak occurred during the dry season. For the same reason described by Ichii *et al.* (2007), the default soil depth in LPJ of 1.5 m was too shallow and needed to be adjusted.

Hydraulic redistribution is another mechanism that regulates soil moisture sensitivity in the Amazon forest (Lee *et al.*, 2005), explaining why satellite observations did not show a clear impact on vegetation condition as a result of the severe drought recorded in 2005 (Saleska *et al.*, 2003), when the rainfall recorded in the Solimões river basin was $100\,\mathrm{mm\,month^{-1}}$ lower than normal from May to September. However, none of the three models provides a mechanism for hydraulic redistribution. This is another reason that the critical annual precipitation amount should be set at $<1500\,\mathrm{mm\,yr^{-1}}$ in the western Amazon.

Annual NPP increases linearly in response to increases in shortwave radiation both in Biome-BGC and LPJ (Fig. 10c). It has been reported that the efficiency of photosynthesis is higher under diffuse radiation than direct radiation (Gu *et al.*, 2003). But, using model simulations, Alton *et al.* (2007) reported that enhancement of LUE cannot compensate the decrease of total amount of shortwave radiation for dense canopy forests. Thus, the conclusion that NPP increase were caused by the increase of shortwave radiation cannot be affected by considering fraction of diffusive irradiance to total shortwave radiation. Furthermore, diffuse irradiance caused by the aerosols from biomass burning on cloud free days (Oliveira *et al.*, 2007) can support a linearly increasing response in NPP to shortwave radiation. Compare with cloud scattering, aerosol scattering make smaller change in the total amount of shortwave radiation because of the characteristic of more forward scattering (Alton *et al.*, 2007).

CO_2 fertilization effect vs. shortwave radiation

Nemani *et al.* (2003) explained an observed positive trend in NPP over the Amazon region with a corresponding increase in shortwave radiation. Lewis *et al.* (2004b) suggested that the biomass increase could be due to the CO_2 fertilization effect and/or an increase in shortwave radiation, because the biomass increase was observed everywhere at the continental scale, while other climate variables did not show spatially consistent trends at such a wide scale. Our results from the Biome-BGC and LPJ simulations suggest that shortwave radiation, rather than the CO_2 fertilization effect, increases in temperature, or changes in precipitation, explain the seasonal positive trends in NDVI observed from August to December over the study period. In the model simulations, the increase in NPP resulting from the CO_2 fertilization effect was higher than the radiation-driven increase. The increase in NPP caused by the CO_2 fertilization effect can be overestimated because a strong dependency of light use efficiency upon temperature is hypothesized in Farquhar models (Hickler *et al.*, 2008). In the Free Air CO_2 Enrichment (FACE) experiment, CO_2 fertilization did not increase LAI, although NPP increased as a result of enhanced light use efficiency (Norby *et al.*, 2005). While the FACE experiment was not conducted in the tropics, it demonstrated that it is possible that increases in NPP resulting from CO_2 fertilization cannot be detected by NDVI. Biome-BGC and LPJ did not consider such an allometric change corresponding to elevated CO_2 concentrations, and it is possible that the modeled increase in NPP resulting from CO_2 fertilization did not show up in the monthly trend in AVHRR NDVI because additional carbon was allocated to nonleaf biomass. Therefore, our results do not exclude the possibility of a CO_2 fertilization effect on tropical rainforests in the Amazon.

However, some issues still remain that both Biome-BGC and LPJ cannot resolve. For example, both models cannot explain some of the other effects mediated by elevated atmospheric CO_2 concentration, such as mineral nutrient availability, growth of lianas, and biodiversity effects, which are also critical for predicting ecosystem response in a CO_2-rich world (Körner, 2004). Furthermore, other nutrients (e.g. nitrogen, potassium, and phosphorus) can limit the growth of vegetation in response to the CO_2 fertilization effect, complicating the full capture of nutrient cycles by ecosystem models (Hungate *et al.*, 2003). These factors should be considered for future research and modeling in the Amazon region.

Conclusions

In this study, we analyzed the trends in photosynthetic activity in the western Amazon over the last two decades to explain the observed NDVI trend through the use of modeling experiments driven by multiple climate datasets. The positive trend in GIMMS NDVI was found to be primarily influenced by increases in NDVI from August to December. We analyzed the trends of climate variables from multiple datasets for the period from 1984 to 2002, finding the trend in each climatic parameter to vary depending on the dataset. Among the temperature datasets, a significant positive

trend was found in the CRU dataset. Among the precipitation datasets, the GPCP dataset showed a significant positive trend and NCEP showed a significant negative trend, while no significant trend could be found in the CRU and UD datasets. Shortwave radiation data showed increasing trends, while cloud cover showed negative trends in both the ISCCP and NCEP datasets.

We then used the different climate datasets to drive three ecosystem models (CASA, Biome-BGC, and LPJ) to simulate the trends in GIMMS NDVI by modeling NPP. CO_2 fertilization effects were evenly distributed over the course of an entire year, but NDVI did not show such an overall increase. Our results do not exclude the possibility that potential gains in productivity resulting from CO_2 fertilization effects were not likely distributed to leaf production; however, we suggest that changes in climate rather than CO_2 fertilization effects could explain the increasing trend in NDVI. Specifically, a positive trend in shortwave radiation and negative trend in cloud cover most strongly explain the corresponding increase in NDVI, as our simulations showed that these factors drove a simulated increase in NPP for the same months (from August to December) in which the increases in NDVI have been observed.

Acknowledgement

This research was funded by grants from NASA Earth Sciences program.

References

Adler RF, Huffman GJ, Chang A *et al*. (2003) The version-2 Global Precipitation Climatology Project (GPCP) monthly precipitation analysis (1979-present). *Journal of Hydrometeorology*, **4**, 1147–1167.

Alton PB, North PR, Los SO (2007) The impact of diffuse sunlight on canopy light-use efficiency, gross photosynthetic product and net ecosystem exchange in three forest biomes. *Global Change Biology*, **13**, 776–787.

Asner GP, Knapp DE, Broadbent EN, Oliveira PJC, Keller M, Silva JN (2005) Selective logging in the Brazilian Amazon. *Science*, **310**, 480–482.

Baker TR, Phillips OL, Malhi Y *et al*. (2004) Increasing biomass in Amazonian forest plots. *Philosophical Transactions of the Royal Society, Series B*, **359**, 353–365.

Ball JT, Woodrow IE, Berry JA (1987) A model predicting stomatal conductance and its contribution to the control of photosynthesis under different environmental conditions. In: *Progress in Photosynthesis Research*, Vol. 4 (ed. Biggins J), pp. 221–224. Martinus Nijhoff, Dordrecht.

Barkstrom BR (1984) The Earth Radiation Budget Experiment (ERBE). *Bulletin of the American Meteorological Society*, **65**, 1170–1185.

Carswell FE, Costa AL, Palheta M *et al*. (2002) Seasonality in CO_2 and H_2O flux at an eastern Amazonian rain forest. *Journal of Geophysical Research*, **107**, 8076.

Chagnon FJF, Bras RL (2005) Contemporary climate change in the Amazon. *Geophysical Research Letters*, **32**, L13703.

Chagnon FJF, Bras RL, Wang J (2004) Climatic shift in patterns of shallow clouds over the Amazon. *Geophysical Research Letters*, **31**, L24212.

Chen J, Carlson BE, Del Genio AD (2002) Evidence for strengthening of the tropical general circulation in the 1990s. *Science*, **295**, 838–841.

Cramer W, Bondeau A, Schaphoff S, Luchet W, Smith B, Sitch S (2004) Tropical forests and the global carbon cycle: impacts of atmospheric carbon dioxide, climate change and rate of deforestation. *Philosophical Transactions of the Royal Society, Series B*, **359**, 331–343.

Cramer W, Kichlighter DW, Bondeau A *et al*. (1999) Comparing global models of terrestrial Net Primary Productivity (NPP): overview and key results. *Global Change Biology*, **5**, 1–15.

De Marsily G (1986) *Quantitative Hydrogeology: Groundwater Hydrology for Engineers*. Academic Press, New York.

Evan AT, Heidinger AK, Vimont DJ (2007) Arguments against a physical long-term trend in global ISCCP cloud amounts. *Geophysical Research Letters*, **34**, L04701.

Farquhar GD, von Caemmerer S, Berry JA (1980) A biochemical model of photosynthetic CO_2 assimilation in leaves of C_3 species. *Planta*, **149**, 78–90.

Fekete BM, Vörösmarty CJ, Roads JO, Willmott CJ (2004) Uncertainties in precipitation and their impacts on runoff estimates. *Journal of Climate*, **17**, 294–304.

Gerten D, Schaphoff S, Haberlandt U, Lucht W, Sitch S (2004) Terrestrial vegetation and water balance – hydrological evaluation of a dynamic global vegetation model. *Journal of Hydrology*, **286**, 249–270.

Grace J, Lloyd J, McIntyre J *et al*. (1995) Carbon dioxide uptake by an undisturbed tropical rain forest in southwest Amazonia, 1992 to 1993. *Science*, **270**, 778–780.

Gu L, Baldocchi DD, Wofsy SC, Munger JW, Michalsky JJ, Urbanski SP, Boden TA (2003) Response of a deciduous forest to the Mount Pinatubo eruption: enhanced photosynthesis. *Science*, **299**, 2035–2038.

Gurney KR, Law RM, Denning AS *et al*. (2002) Towards robust regional estimates of CO_2 sources and sinks using atmospheric transport models. *Nature*, **415**, 626–630.

Haxeltine A, Prentice IC (1996) A general model for the light-use efficiency of primary production. *Functional Ecology*, **10**, 551–561.

Helsel DR, Hirsch RM (1992) *Statistical Methods in Water Resources*. Elsevier, Amsterdam.

Hicke JA (2005) NCEP and GISS solar radiation data sets available for ecosystem modeling: description, differences, and impacts on net primary production. *Global Biogeochemical Cycles*, **19**, GB2006.

Hickler T, Smith B, Prentice IC, Mjöfors K, Miller P, Arneth A, Sykes MT (2008) CO_2 fertilization in temperate FACE experiments not representative of boreal and tropical forests. *Global Change Biology*, **14**, 1531–1542.

Published 2009

Houghton RA, Skole DL, Nobre CA, Hackler JL, Lawrence KT, Chomentowski WH (2000) Annual fluxes of carbon from deforestation and regrowth in the Brazilian Amazon. *Nature*, **403**, 301–304.

Huete AR, Didan K, Shimabukuro YE *et al*. (2006) Amazon rainforests green-up with sunlight in dry season. *Geophysical Research Letters*, **33**, L06405.

Hungate BA, Dukes JS, Shaw MR, Luo Y, Field CB (2003) Nitrogen and climate change. *Science*, **302**, 1512–1513.

Hutyra LR, Munger JW, Saleska SR *et al*. (2007) Seasonal controls on the exchange of carbon and water in an Amazonian rain forest. *Journal of Geophysical Research*, **112**, G03008.

Ichii K, Hashimoto H, Nemani R, White M (2005) Modeling the interannual variability and trends in gross and net primary productivity of tropical forests from 1982 to 1999. *Global and Planetary Change*, **48**, 274–286.

Ichii K, Hashimoto H, White MA *et al*. (2007) Constraining rooting depths in tropical rainforests using satellite data and ecosystem modeling for accurate simulation of gross primary production seasonality. *Global Change Biology*, **13**, 67–77.

Jarvis PJ (1976) The interception of the variations in leaf water potential and stomatal conductance found in canopies in the field. *Philosophical transactions of the Royal Society of London. Series B*, **273**, 593–610.

Kalnay E, Kanamitsu M, Kistler R *et al*. (1996) The NCEP/NCAR 40-year reanalysis project. *Bulletin of the American Meteorological Society*, **77**, 437–471.

Kendall MG (1938) A new measure of rank correlation. *Biometrika*, **30**, 81–93.

Kobayashi H, Dye DG (2005) Atmospheric conditions for monitoring the long-term vegetation dynamics in the Amazon using normalized difference vegetation index. *Remote Sensing of Environment*, **97**, 519–525.

Körner C (2004) Through enhanced tree dynamics carbon dioxide enrichment may cause tropical forests to lose carbon. *Philosophical Transactions of the Royal Society, Series B*, **359**, 493–498.

Lee J-E, Oliveira RS, Dawson TE, Fung I (2005) Root functioning modifies seasonal climate. *Proceedings of the National Academy of Science of the United States of America*, **102**, 17576–17581.

Legates DR, Willmott CJ (1990a) Mean seasonal and spatial variability in gauge-corrected, global precipitation. *International Journal of Climatology*, **10**, 111–127.

Legates DR, Willmott CJ (1990b) Mean seasonal and spatial variability in global surface air temperature. *Theoretical and Applied Climatology*, **41**, 11–21.

Lewis SL, Malhi Y, Phillips OL (2004a) Fingerprinting the impacts of global change on tropical forests. *Philosophical Transactions of the Royal Society of London. Series B: Biological Sciences*, **359**, 437–462.

Lewis SL, Phillips OL, Baker TR *et al*. (2004b) Concerted changes in tropical forest structure and dynamics: evidence from 50 South American long-term plots. *Philosophical Transactions of the Royal Society, Series B*, **359**, 421–436.

Malhi Y (2008) Climate change, deforestation, and the fate of the Amazon. *Science*, **319**, 169–172.

Malhi Y, Nobre AD, Grace J, Kruijt B, Pereira MGP, Culf A, Scott S (1998) Carbon dioxide transfer over a central Amazonian rain forest. *Journal of Geophysical Research*, **103**, 31593–31612.

Malhi Y, Pegoraro E, Nobre AD, Pereira MGP, Grace J, Culf AD, Clement R (2002) Energy and water dynamics of a central Amazonian rain forest. *Journal of Geophysical Research*, **107**, 8061.

Malhi Y, Wright J (2004) Spatial patterns and recent trends in the climate of tropical rainforest regions. *Philosophical Transactions of the Royal Society, Series B*, **359**, 311–329.

Marengo JA (2004) Interdecadal variability and trends of rainfall across the Amazon basin. *Theoretical and Applied Climatology*, **78**, 79–96.

Marengo JA, Nobre CA, Tomasella J *et al*. (2008) The drought of Amazonia in 2005. *Journal of Climate*, **21**, 495–516.

Mitchell TD, Jones PD (2005) An improved method of constructing a database of monthly climate observations and associated high-resolution grids. *International Journal of Climatology*, **25**, 693–712.

Monteith JL (1972) Solar radiation and productivity in tropical ecosystems. *Journal of Applied Ecology*, **9**, 747–766.

Myneni RB, Yang W, Nemani RR *et al*. (2007) Large seasonal swings in leaf area of Amazon rainforests. *Proceedings of the National Academy of Sciences*, **104**, 4820–4823.

Nemani RR, Keeling CD, Hashimoto H *et al*. (2003) Climate driven increase in terrestrial net primary production from 1982 to 1999. *Science*, **300**, 1560–1563.

Nepstad DC, de Carvalho CR, Davidson EA *et al*. (1994) The role of deep roots in the hydrological and carbon cycles of Amazonian forests and pastures. *Nature*, **42**, 61–65.

Norby RJ, DeLucia EH, Gielen B *et al*. (2005) Forest response to elevated CO_2 is conserved across a broad range of productivity. *Proceedings of the National Academy of Sciences of the United States of America*, **102**, 18052–18056.

Oliveira PHF, Artaxo P, Pires C *et al*. (2007) The effects of biomass burning aerosols and clouds on the CO_2 flux in Amazonia. *Tellus B*, **59**, 338–349.

Ometto JPHB, Nobre AD, Rocha HR, Artaxo P, Martinelli LA (2005) Amazonia and the modern carbon cycle: lessons learned. *Oecologia*, **143**, 483–500.

Phillips OL, Baker TR, Arroyo L *et al*. (2004) Pattern and process in Amazon tree turnover, 1976–2001. *Philosophical Transactions of the Royal Society, Series B*, **359**, 381–407.

Pinzón JE, Brown ME, Tucker CD (2005) EMD correction of orbital drift artifacts in satellite data stream. In: *The Hilbert-Huang Transform and Its Applications* (eds Huang NE, Shen SSP), pp. 167–186. World Scientific Publishers, Singapore.

Potter CS, Randerson JT, Field CB, Matson PA, Vitousek PM, Mooney HA, Klooster SA (1993) Terrestrial ecosystem production: a process model based on global satellite and surface data. *Global Biogeochemical Cycles*, **7**, 811–841.

Salati E, Vose PB (1984) Amazon basin: a system in equilibrium. *Science*, **225**, 129–138.

Saleska SR, Miller SD, Matross DM *et al*. (2003) Carbon in Amazon forests: unexpected seasonal fluxes and disturbance-induced losses. *Science*, **302**, 1554–1557.

Schloss AL, Kicklighter DW, Kaduk J *et al*. (1999) Comparing global models of terrestrial Net Primary Productivity (NPP): comparison of NPP to climate and the Normalized

Difference Vegetation Index (NDVI). *Global Change Biology*, **5**, 25–34.

Sitch S, Smith B, Prentice IC *et al*. (2003) Evaluation of ecosystem dynamics, plant geography and terrestrial carbon cycling in the LPJ dynamic vegetation model. *Global Change Biology*, **9**, 161–185.

Stanhill G, Cohen S (2001) Global dimming: a review of the evidence for a widespread and significant reduction in global radiation with discussion of its probable causes and possible agricultural consequences. *Agricultural and Forest Meteorology*, **107**, 255–278.

Thornton PE, Law BE, Gholz HL *et al*. (2002) Modeling and measuring the effects of disturbance history and climate on carbon and water budgets in evergreen needleleaf forests. *Agricultural and Forest Meteorology*, **113**, 185–222.

Tian H, Melillo JM, Kicklighter DW, McGuire AD, Helfrich JVK III, Moore B III, Vörösmarty CJ (1998) Effect of interannual climate variability on carbon storage in Amazonian ecosystems. *Nature*, **396**, 664–667.

Tucker CJ, Pinzon JE, Brown ME *et al*. (2005) An extended AVHRR 8-km NDVI dataset compatible with MODIS and SPOT Vegetation NDVI data. *International Journal of Remote Sensing*, **26**, 4485–4498.

Victoria RL, Martinelli LA, Moraes JM *et al*. (1998) Surface air temperature variations in the Amazon region and its borders during this century. *Journal of Climate*, **11**, 1105–1110.

Wielicki BA, Barkstrom BR, Harrison EF, Lee RB, Louis Smith G, Cooper JE (1996) Clouds and the Earth's Radiant Energy System (CERES): an earth observing system experiment. *Bulletin of the American Meteorological Society*, **77**, 853–856.

Wielicki BA, Wong T, Allan RP *et al*. (2002) Evidence for large decadal variability in the tropical mean radiative energy budget. *Science*, **295**, 841–844.

Wild M, Gilgen H, Roesch A *et al*. (2005) From dimming to brightening: decadal changes in solar radiation at earth's surface. *Science*, **308**, 847–850.

Willmott CJ, Matsuura K (2001) Terrestrial air temperature and precipitation: Monthly and annual time series (1950–1999) version 1.02. Available at http://climate.geog.udel.edu/ ~ climate/html_pages/README.ghcn_ts2.html (access date: 04/02/2009).

Zhang Y, Rossow WB, Lacis AA, Oinas V, Mishchenko MI (2004) Calculation of radiative fluxes from the surface to top of atmosphere based on ISCCP and other global data sets: refinements of the radiative transfer model and the input data. *Journal of Geophysical Research*, **109**, D19105.

Zhao M, Running SW, Nemani RR (2006) Sensitivity of Moderate Resolution Imaging Spectroradiometer (MODIS) terrestrial primary production to the accuracy of meteorological reanalyses. *Journal of Geophysical Research*, **111**, G01002.

Published 2009
